www.cadanda.com
Computer-Aided Design AND APPLICATIONS

High-quality Approximation Technique for Two G^1-continuous Offset Surfaces

Naoyuki Satoh[1], Katsutsugu Matsuyama[2], Kouichi Konno[3] and Yoshimasa Tokuyama[4]

[1]Iwate University, t5810003@iwate-u.ac.jp
[2]Iwate University, kmatsu@iwate-u.ac.jp
[3]Iwate University, konno@cis.iwate-u.ac.jp
[4]Tokyo Polytechnic University, tokuyama@t-kougei.ac.jp

ABSTRACT

This paper proposes a technique for approximating two G^1-continuous offset surfaces. Since offset surfaces are in general not rational representation, spline approximations of offset surfaces are widely used. However, when two G^1-continuous offset surfaces are approximated using existing methods, the shape data quality is reduced because gaps or creases arise between two approximated surfaces. Our technique generates two G^1-continuous approximated surfaces represented by C^1-continuous bicubic B-spline surfaces. The approximated surfaces are higher quality than those generated using existing methods, because no gaps or creases arise between those surfaces.

Keywords: offset surface, surface approximation, G^1-continuity, C^1-continuity.

1. INTRODUCTION

Surface offset is an important operation in CAD and various applications, such as NC machining, tolerance analysis, or robotics. Since the face of a three-dimensional model is usually constructed by multiple rational parametric surfaces, offset surfaces are required for the operation. An offset surface is defined as a locus of points obtained by moving all points of the original surface at constant distance along the direction of the unit normal vector of the surface at each of the points. If two surfaces are G^1-continuous, the offset surfaces of those are also G^1-continuous [6]. However, a spline approximation of offset surfaces is widely used because offset surfaces are in general not rational representation, except for special cases such as analytic surfaces [1,11].

Offset surfaces are often given to numerical calculation of first order differential equations, such as trace calculations for blending surfaces or tracing intersection between surfaces [5,12]. Thus, approximated surfaces are tractable if they are at least C^1-continuous. Several methods for approximating offset surfaces with at least C^1-continuous spline surfaces have already been presented [4,7,14]. The methods can approximate offset surfaces with piecewise bicubic surface patches which are tractable since those are low degree. However, none of those methods consider the continuity of adjacent offset surfaces because they generate offset surfaces individually. Therefore, gaps or creases arise between two approximated surfaces when two G^1-continuous offset surfaces are approximated using the methods. G^1-discontinuity caused by such as gaps or creases reduces shape data quality because it incurs data conversion failure [9,10].

Thus, this paper proposes a technique for a C^1 spline approximation of offset surfaces considering continuity of adjacent offset surfaces. Our technique can generate approximated offset surfaces which are higher quality than existing methods because no gaps or creases arise between approximated surfaces, when two G^1-continuous offset surfaces are approximated.

The remainder of the paper is organized as follows: In Section 2 we study the existing methods of C^1 spline approximation of offset surfaces, and reveal details of the reason that gaps or creases arise between two approximated surfaces, when two G^1-continuous offset surfaces are approximated using the methods. Section 3 give the algorithm of our technique for approximating two G^1-continuous offset surfaces without gaps or creases between two

Computer-Aided Design & Applications, 11(1), 2013, 78–89, http://dx.doi.org/10.1080/16864360.2013.834146

Taylor & Francis

approximated surfaces. Section 4 illustrates some examples using practical models. Finally, in Section 5 we conclude this paper.

2. EXISTING METHODS

Farouki [4] approximates offset surfaces with piecewise bicubic Hermite interpolation patches. The patches are applied to n^2 square areas obtained by subdividing the parameter domain of offset surfaces so that u and v directions are divided into n sections uniformly. Then, the parameter domain is subdivided until all the patches satisfy a given tolerance. Positions, partial derivatives and twist vectors at four corners in each of the patches are coincident with those of the exact offset surface. Control points of the patches except these ones on the four corners are calculated by Hermite interpolation using these properties. Thus, the adjacent patches are C^1-continuous. However, the [4] does not consider continuity of adjacent offset surfaces because it generates offset surfaces individually. When two G^1-continuous offset surfaces are approximated using the method [4], creases arise between two approximated offset surfaces because G^1-continuity are not guaranteed between the surfaces, although no gap arises between those if the number of divisions is equalized in each of the parameter domains of the offset surfaces. Fig. 1(a) and (b) show an example of such a situation where creases arise between two approximated surfaces. Fig. 1(a) shows two approximated offset surfaces including creases. Each surface consists of 2^2 patches. Fig. 1(b) is the enlarged view of Fig. 1(a) along the common boundary curve between two surfaces (or referred to as the common boundary in the following description), and shows normal vectors of the surfaces along boundary curves. As shown in Fig. 1(b), creases between two surfaces are appeared. Therefore, the method [4] reduces shape data quality because creases arise as shown in Fig. 1(b).

Hoschek [7] approximates offset surfaces with piecewise bicubic Bezier patches. The patches are applied to each rectangular area obtained by subdividing a parametric domain of an offset surface along u and v directions. Then, the parametric domain is subdivided until all the patches satisfy a given tolerance. In addition, subdivision points in the parametric domain depend on the shape of the offset surface. Positions and directions of partial derivative vectors at four corners of each of the patches are coincident with those of the exact offset surface. Control points of the patches except for those on the four corners are calculated using the least-squares method using sample points chosen with equidistant parameter values in the parametric domain to be approximated. Continuity between adjacent patches is C^1 because neighboring patches are given a constraint of C^1-continuity. However, the [7] does not consider continuity of adjacent offset surfaces because it generates offset surfaces individually. When two G^1-continuous offset surfaces are approximated using the method [7], in parametric domains of the surfaces, division points on the common boundary between the surfaces as the result of subdivision are not coincident each other. This is because the subdivision depends on the shape of an offset surface, that is, the shapes of two boundary curves of the approximated surfaces on the common boundary are not same in general. Thus, gaps arise between two approximated surfaces. The portion in an oval with a broken line in Fig. 1(c) is an example of gaps. Therefore, the method [7] reduces shape data quality because gaps arise as shown in Fig. 1(c).

Piegl and Tiller [14] approximate offset surfaces with a bicubic B-spline surface. First, a large number of sample points are extracted for equally spaced parameters on an offset surface. The number of the sample points depends on the shape of the offset surface. Next, a bicubic B-spline surface that has the same number of control points as the sample points is generated by interpolating the sample points. Finally, these control points are reduced by removing as many knots as possible in the range of a given tolerance. Continuity between adjacent patches of the B-spline surface is C^2. However, the [14] does not consider

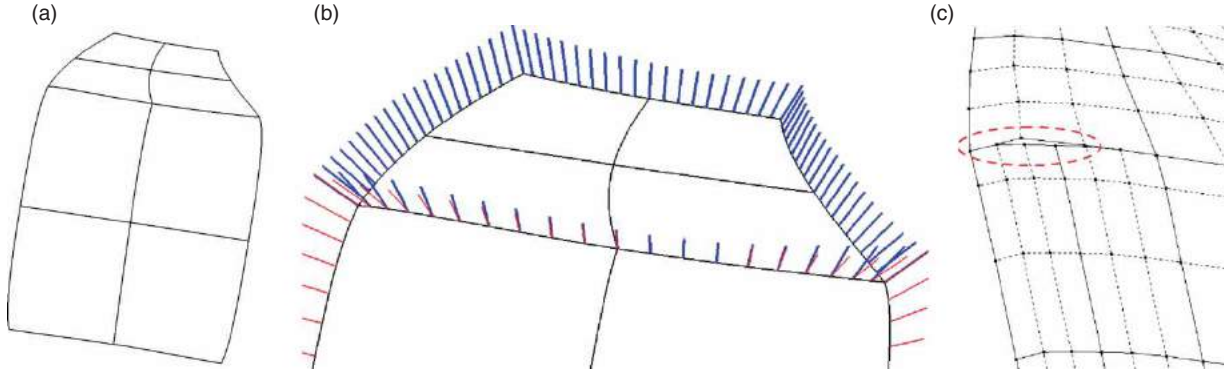

Fig. 1: (a) Two approximated surfaces with creases, (b) Enlarged view of (a) with normal vectors, (c) A gap between two approximated surfaces.

continuity of adjacent offset surfaces because it generates offset surfaces individually. When two G^1-continuous offset surfaces are approximated using the method [14], the number of sample points on the common boundary between two offset surfaces is not equal generally since it depends on the shape of an offset surface, that is, the shapes of two boundary curves of the approximated surfaces on the common boundary are not the same in general. Thus, gaps arise between two approximated surfaces. Therefore, the method [14] reduces shape data quality.

As described in this section, when two G^1-continuous offset surfaces are approximated using existing methods [4,7,14], shape data quality is reduced because gaps or creases arise between two approximated offset surfaces. Thus, this paper proposes a technique of high-quality approximation for two G^1-continuous offset surfaces by avoiding such as gaps or creases.

3. THE APPROXIMATION OF TWO G^1-CONTINUOUS OFFSET SURFACES

3.1. Outline of the Algorithm

To avoid gaps or creases that reduce shape data quality, we propose a technique for approximating two G^1-continuous offset surfaces that generates two G^1-continuous approximated surfaces represented by C^1-continuous bicubic B-spline surfaces. First, approximate each of the offset surfaces with piecewise bicubic Bezier patches. The patches are generated so that two adjacent those are C^1-continuous except those existing along the common boundary. Then, if the patches are not adjoining to be one-on-one on the common boundary as the result of the approximation, subdivide the parameter domains so that two sets of division points along the parameter interval of the common boundary coincide with each other. The details of this procedure are described in Section 3.2. Next, adjust control points of the patches existing along the common boundary so that two adjacent those on the common boundary are G^1-continuous and those along the common boundary are C^1-continuous. To these control points, our original two constraint conditions which enable patches to satisfy G^1- and C^1-continuity simultaneously are given, in addition to the constraint conditions guaranteeing G^1- and C^1-continuity individually. The details of this procedure are described in Section 3.3. Finally, generate two C^1 bicubic B-spline surfaces by combining the patches. As the result, no gaps or creases arise because two approximated surfaces are G^1-continuous.

3.2. Approximating Offset Surfaces with Piecewise Bicubic Bezier Patches

To approximate two G^1-continuous offset surfaces with two C^1 spline surfaces, we approximate each of the offset surfaces with piecewise bicubic Bezier patches while considering continuity of adjacent patches. The approximation procedure consists of the four steps: approximating an offset surface with a bicubic Bezier patch (Step 1), measuring errors and subdividing the patch (Step 2), joining the patches with C^1-continuity (Step 3), and joining the patches one-on-one on the common boundary (Step 4).

Step 1: We approximate an offset surface with a bicubic Bezier patch. Control points on boundary curves of the patch and inner control points of the patch are calculated separately in a similar manner to Hoschek's method [7]. Control points on boundary curves are obtained by approximating boundary curves of the offset surface with cubic Bezier curves. The cubic Bezier curves are calculated using the least-squares method using sample points on boundary curves of the offset surface [7], while initial points and directions of tangent vectors of the cubic Bezier curves at both end points are constrained to be coincident with ones of boundary curves of the offset surface. These sample points occur at corners of polylines approximating boundary curves of the offset surface adaptively; that is, sample points are obtained at subdivision points in parameter intervals of boundary curves of the offset surface (black dots in Fig. 2(a) are an example). First, in a parameter interval, we divide a boundary curve of the offset surface into four equal sections, and then check if each curve segment can be regarded as a straight line segment. If an angle between two tangent vectors of a curve segment at both end points is regarded as zero in a range of a given tolerance (or referred to as the angle tolerance in the following description), the curve segment is regarded as a line segment. Next, in the parameter interval, we bisect the curve segments that are not regarded as line segments, and then check if each curve segment after the bisection can be regarded as a straight line segment. These procedures are repeated until all curve segments are regarded as straight line segments. Meanwhile, inner control points of the patch are calculated using the least-squares method using sample points on the offset surface [15]. These sample points occur due to parameter values of all sample points obtained by the calculation of four boundary curves of the patch. To be more specific, sample points are generated at parameter position on the offset surface in each u, v pair obtained from the sample points which were used in the calculation of four boundary curves of the patch, except for parameter values on the boundary curves (white dots in Fig. 2(a) are an example).

Step 2: First, we measure errors of the patch with referencing the standard of geometrical tolerancing of a profiled surface [8]. The standard defines a tolerance zone to be between two envelope surfaces defined by spheres of which a center lies on the theoretical surface and a diameter equals a given tolerance [8]. However, it is difficult to measure errors of the patch at every point successively. We, therefore, measure

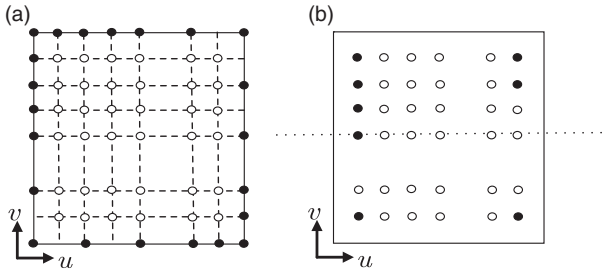

Fig. 2: (a) Sample points on an offset surface, (b) Subdivision of the parameter domain.

errors of the patch discretely. Then, boundary curves of the patch and interior of the patch are measured separately because they are approximated individually. For boundary curves of the patch, we measure a distance between an exact point on a boundary curve of the theoretical offset surface and a point on a boundary curve of the patch, which is nearest to a normal vector of the offset surface at the exact point. To be more specific, for each of sample points which were used to calculate control points on the boundary curves, we calculate a nearest point by using the Newton's method, and check if a distance between the nearest point and the sample point is not greater than a given tolerance. For interior of the patch, we measure a distance between an exact point on the theoretical offset surface and a point on the patch which is nearest to the normal vector of the offset surface at the exact point. To be more specific, for each of the sample points which were used to calculate inner control points of the patch, we calculate a nearest point by using the Newton's method, and check if a distance between the nearest point and the sample point is not greater than the tolerance. Next, if the nearest point that does not satisfy the tolerance on the boundary curve of the patch exists, we subdivide a parameter domain of the offset surface so that the parameter interval in u or v direction is bisected. If the boundary curve is along u direction, the parameter interval in u direction is bisected. Otherwise, the parameter interval in v direction is bisected. After the subdivision, we generate bicubic Bezier patches in each of the subdivided area in the parameter domain of the offset surface using the method in Step 1. Then, we recursively repeat Step 2 for each patch until all boundary curves of the patches are within the tolerance. Next, if a nearest point not within the tolerance exists, we subdivide the parameter domain of the offset surface so that the parameter interval in either the u or v direction is bisected. The parameter interval to be divided depends on a deviation of the nearest points that are not within the tolerance. More specifically, it depends on difference between the rules of the nearest points that do not satisfy the tolerance in each of two areas generated by bisecting the parameter domain of the patch in either the u or v direction. If the difference in the u direction is greater than at in the v direction, the parameter interval in u direction is bisected. Otherwise, the parameter interval in v direction is bisected. Fig. 2(b) is an example bisection. The black dots are nearest points that are not within tolerance, and the white dots are nearest points that are within tolerance. The dotted line depicted in Fig. 2(b) represents the direction to bisect the parameter domain of the patch. As the result, the parameter domain of the patch is divided into two more precise areas and one less precise area. The possibility that the more precise area is further subdivided is lower than the less precise area. Accordingly, it is expected fewer patches will be generated eventually than in the case when both areas are further subdivided. After each subdivision, we generate bicubic Bezier patches within each of the subdivided areas in the parameter domain of the offset surface using the method in Step 1. We then recursively repeat Step 2 in each of the patches until all patches within the tolerance.

Step 3: If two or more patches are generated in Step 2, we adjust position of control points of the patches, using Beeker's method [4], so that adjacent patches become C^1-continuous except for those along the common boundary. First, two boundary curves of the patches connecting along the u or v direction except for those on the common boundary are adjusted to become C^1-continuous. Two control points adjacent to the connecting point of two boundary curves (bold red dots in Fig. 3(a)) are adjusted while retaining directions of tangent vectors of two boundary curves at the connecting point. Let $\mathbf{b}$ be the connecting point. Let $\mathbf{a}$ and $\mathbf{c}$ be the adjacent control points of $\mathbf{b}$ (see Fig. 3(a)), and let $\tilde{\mathbf{a}}$ and $\tilde{\mathbf{c}}$ be the counterpart control points after the adjustment. $\mathbf{a}$ and $\mathbf{c}$ are adjusted so that they satisfy the following constraints:

$$\tilde{\mathbf{c}} - \mathbf{b} = \mu(\mathbf{b} - \tilde{\mathbf{a}}), \quad \tilde{\mathbf{a}} - \mathbf{b} = \lambda(\mathbf{a} - \mathbf{b}), \tag{3.1}$$

where μ is ratio of parameter intervals of two boundary curves and λ is an unknown scalar. From Eqn.(3.1), $\tilde{\mathbf{a}}$ and $\tilde{\mathbf{c}}$ are expressed by linear functions of λ. Therefore, we determine λ as follows using the least-squares method so that two control points move as little as possible (see APPENDIX for the derivation).

$$\lambda = \frac{|\mathbf{a} - \mathbf{b}|^2 + \mu(\mathbf{a} - \mathbf{b})(\mathbf{b} - \mathbf{c})}{(1 + \mu^2)|\mathbf{a} - \mathbf{b}|^2}. \tag{3.2}$$

$\tilde{\mathbf{a}}$ and $\tilde{\mathbf{c}}$ are calculated by substituting Eqn. (3.2) into Eqn.(3.1). Next, four inner control points adjacent to the point at which corners of four patches converge (bold red dots in Fig. 3(b)) are adjusted. Let $\mathbf{d}$, $\mathbf{e}$, $\mathbf{f}$, and $\mathbf{g}$ be four inner control points, counter-clockwise, starting from the control point nearest to the origin of the parameter domain of the offset surface (see Fig. 3(b)). Let $\tilde{\mathbf{d}}, \tilde{\mathbf{e}}, \tilde{\mathbf{f}}$, and $\tilde{\mathbf{g}}$ be counterpart control points after the adjustment. Let $\mathbf{h}$, $\mathbf{i}$, $\mathbf{j}$, and $\mathbf{k}$ be control points of boundary curves adjacent to the point

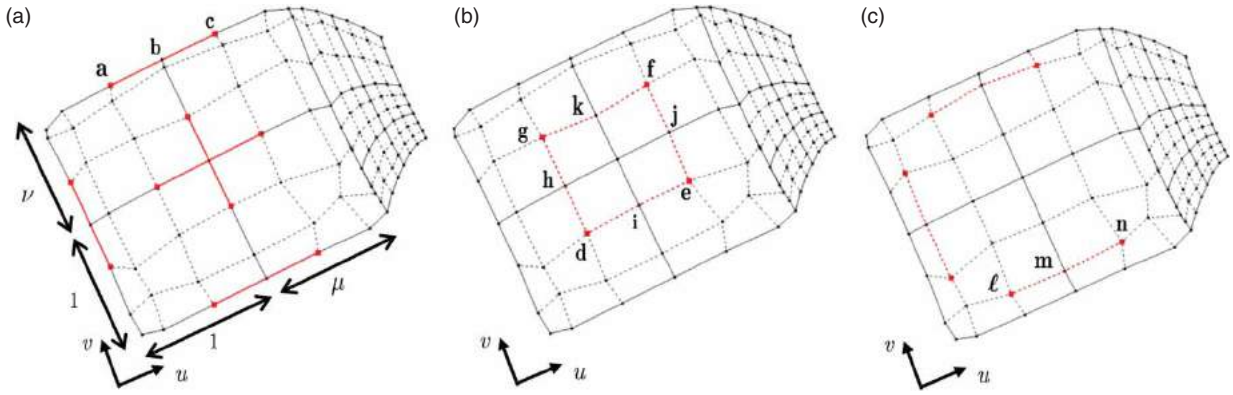

Fig. 3: (a) Two control points adjacent to the connecting point, (b) Four inner control points adjacent to the point at which corners of four patches converge, (c) Two control points adjoining across the boundary curve.

at which corners of four patches converge, counterclockwise, starting from the control point nearest to the v axis of the parameter domain of the offset surface (see Fig. 3(b)). **d**, **e**, **f**, and **g** are adjusted so that they satisfy the following constraints:

$$\tilde{\mathbf{e}} - \mathbf{i} = \mu(\mathbf{i} - \tilde{\mathbf{d}}), \quad \tilde{\mathbf{g}} - \mathbf{h} = \nu(\mathbf{h} - \tilde{\mathbf{d}}),$$
$$\tilde{\mathbf{f}} - \mathbf{k} = \mu(\mathbf{k} - \tilde{\mathbf{g}}), \quad \tilde{\mathbf{f}} - \mathbf{j} = \nu(\mathbf{j} - \tilde{\mathbf{e}}), \tag{3.3}$$

where μ is ratio of parameter intervals of the patches in the u direction and ν is ratio of parameter intervals of the patches in the v direction. From Eqn. (3.3), the simultaneous equations that consist of four equations are derived. However, the solution of the system is indefinite because of rank deficiency. On the other hand, $\tilde{\mathbf{e}}$, $\tilde{\mathbf{f}}$, and $\tilde{\mathbf{g}}$ are expressed as linear functions of $\tilde{\mathbf{d}}$ from Eqn.(3.3). Therefore, we determine $\tilde{\mathbf{d}}$ as follows using the least-squares method so that four control points move as little as possible (see APPENDIX for the derivation).

$$\tilde{\mathbf{d}} = \frac{\mathbf{d} + \mu\{(1+\mu)\mathbf{i} - \mathbf{e}\} + \nu\{(1+\nu)\mathbf{h} - \mathbf{g}\} + \mu\nu\{\mu(1+\nu)\mathbf{h} - (1+\mu)\mathbf{k} + \mathbf{f}\}}{1 + \mu^2 + \nu^2 + \mu^2\nu^2}. \tag{3.4}$$

$\tilde{\mathbf{e}}$, $\tilde{\mathbf{f}}$, and $\tilde{\mathbf{g}}$ are calculated by substituting Eqn.(3.4) into Eqn.(3.3). Next, two inner control points existing beside the boundary curve of the offset surface except for the common boundary and existing across the control point of a boundary curve shared by two patches (bold red dots in Fig. 3(c)) are adjusted. Let ℓ and **n** be two inner control points, and let **m** be the control point of the boundary curve between ℓ and **n** (see Fig. 3(c)). Let $\tilde{\ell}$ and $\tilde{\mathbf{n}}$ be the counterpart control points after the adjustment. ℓ and **n** are adjusted so that they satisfy the following constraints

$$\tilde{\mathbf{n}} - \mathbf{m} = \mu(\mathbf{m} - \tilde{\ell}), \tag{3.5}$$

where μ is ratio of parameter intervals of two patches along the boundary curve of the offset surface. From Eqn.(3.5), $\tilde{\mathbf{n}}$ is expressed by a linear function of $\tilde{\ell}$. Therefore, we determine $\tilde{\ell}$ as follows using the least-squares method so that two control points move as little as possible (see APPENDIX for the derivation).

$$\tilde{\ell} = \frac{\ell + \mu\{(1+\mu)\mathbf{m} - \mathbf{n}\}}{1 + \mu^2}. \tag{3.6}$$

$\tilde{\mathbf{n}}$ is calculated by substituting Eqn.(3.6) into Eqn.(3.5). Finally, we measure errors of each patch using the method in Step 2. If the patches which exceed the tolerance are detected, we subdivide the parameter domain of the offset surface and generate bicubic Bezier patches using the method in Step 2. After that, we repeat Step 3.

Step 4: After the procedure from Step 1 to Step 3 is applied to two offset surfaces, some of bicubic Bezier patches on both offset surfaces are adjacent to the common boundary. If the patches are not adjoining each other to be one-on-one on the common boundary, we subdivide parameter domains of the offset surfaces so that segmentations of parameter intervals along the common boundary in two parameter domains coincide with each other (bold red line in Fig. 4(a) is an example). Then, if the number of segments of the common boundary is smaller than three, we subdivide both parameter domains to prepare for the procedure described in Section 3.3 so that the parameter intervals are divided into four equal sections (bold red line in Fig. 4(b) is an example). Then, we approximate each subdivided area with a bicubic Bezier patch using the method in Step 1. Then, we adjust adjacent patches to become C^1-continuous using the method in Step 3. As the result, four or more couples of patches on the common boundary are generated. Moreover, two adjacent boundary curves on the common boundary in each couple of the patches have same shape because two curves are calculated, using the methods in Step 1 and in Step 3, and using same input and procedure.

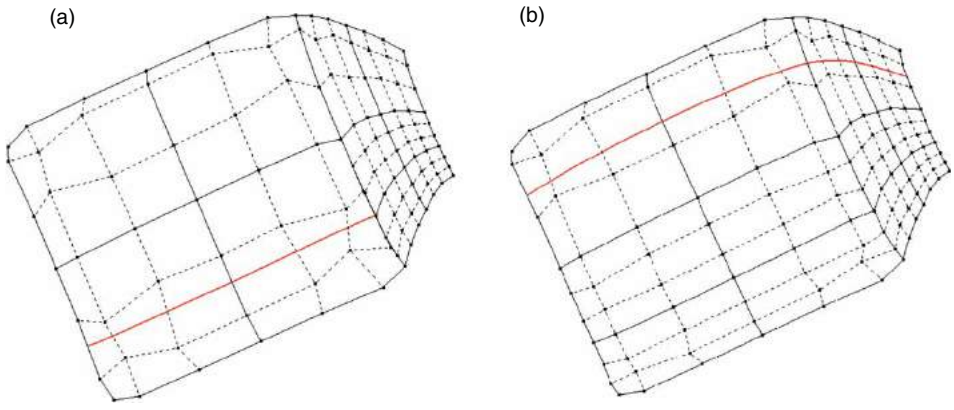

Fig. 4: (a) Subdivide parameter domain so that the patches adjoin one-on-one on the common boundary, (b) Subdivide parameter domains to increase patches on the common boundary.

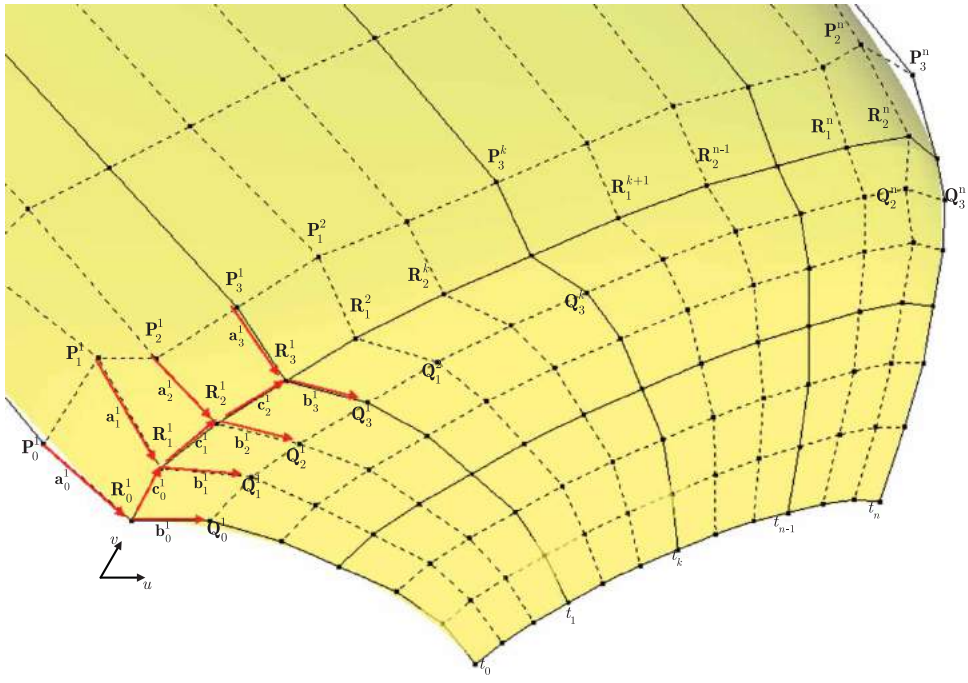

Fig. 5: Patches along the common boundary.

3.3. Adjusting Control Points of Patches Existing Along the Common Boundary

3.3.1. Control points to be adjusted and constraint conditions

We adjust control points of patches existing along the common boundary so that two adjacent those on the common boundary are G^1-continuous and those along the common boundary are C^1-continuous. To describe this technique in Section 3.3.2, this section presents the control points to be adjusted, constraint conditions for the G^1- and C^1-continuity, and our original constraint conditions that guarantee the G^1- and C^1-continuity simultaneously. Fig. 5 shows patches along the common boundary. The description in this section proceeds according to Fig. 5. Assume two offset surfaces are adjoining along v direction in same order. The $n(\geq 4)$ couples of patches adjoining on the common boundary are indexed as $1, 2, \ldots, n$ in ascending order of v. $\mathbf{P}_j^k$ and $\mathbf{Q}_j^k$ are control points existing beside the common boundary, and $\mathbf{R}_j^k$ are control points on the common boundary, where k is the index of the couples, and j is an index from 0 to 3 in ascending order of v. $\mathbf{R}_j^k$ are common control points between the couple of the patches. Control points to be adjusted are $\mathbf{P}_j^k, \mathbf{Q}_j^k, \mathbf{R}_1^k$, and $\mathbf{R}_2^k$. Let $\tilde{\mathbf{P}}_j^k, \tilde{\mathbf{Q}}_j^k, \tilde{\mathbf{R}}_1^k$, and $\tilde{\mathbf{R}}_2^k$ be counterpart control points after the adjustment. Two control points in each of $\mathbf{P}_3^k\ \mathbf{P}_0^{k+1}, \mathbf{Q}_3^k\ \mathbf{Q}_0^{k+1}$,

and $\mathbf{R}_3^k$ $\mathbf{R}_0^{k+1}$ are identical. The same can be said in each of the control points after the adjustment. $\mathbf{a}_j^k, \mathbf{b}_j^k$, and $\mathbf{c}_\ell^k (\ell = 0,1,2)$ are vectors between $\mathbf{R}_j^k$ and its adjacent control point, i.e. $\mathbf{a}_j^k = \mathbf{R}_j^k - \mathbf{P}_j^k, \mathbf{b}_j^k = \mathbf{Q}_j^k - \mathbf{R}_j^k$, and $\mathbf{c}_\ell^k = \mathbf{R}_{\ell+1}^k - \mathbf{R}_\ell^k$. Let $\tilde{\mathbf{a}}_j^k$, $\tilde{\mathbf{b}}_j^k$, and $\tilde{\mathbf{c}}_\ell^k (\ell = 0,1,2)$ be counterpart vectors after the adjustment. $t_k (k = 0,1,\ldots,n)$ are parameter values at corners of the patches on the common boundary in the direction of v.

The constraint condition of C^1-continuity [2] is given by:

$$\begin{aligned}
&\tilde{\mathbf{P}}_1^{k+1} - \tilde{\mathbf{P}}_3^k = \nu_k(\tilde{\mathbf{P}}_3^k - \tilde{\mathbf{P}}_2^k),\\
&\tilde{\mathbf{Q}}_1^{k+1} - \tilde{\mathbf{Q}}_3^k = \nu_k(\tilde{\mathbf{Q}}_3^k - \tilde{\mathbf{Q}}_2^k),\\
&\tilde{\mathbf{R}}_1^{k+1} - \mathbf{R}_3^k = \nu_k(\mathbf{R}_3^k - \tilde{\mathbf{R}}_2^k)\ (k = 1,2,\ldots,n-1) \text{ where}\\
&\qquad\qquad \nu_k = (t_{k+1} - t_k)/(t_k - t_{k-1}). \qquad (3.7)
\end{aligned}$$

The constraint condition of G^1-continuity [3] is given by

$$\begin{aligned}
&\alpha_k(v)\sum_{j=0}^{3} B_j^3(v)\tilde{\mathbf{a}}_j^k + \beta_k(v)\sum_{j=0}^{3} B_j^3(v)\tilde{\mathbf{b}}_j^k\\
&\qquad + \gamma_k(v)\sum_{j=0}^{2} B_j^2(v)\tilde{\mathbf{c}}_j^k = 0\ (k = 1,2,\ldots,n), \qquad (3.8)
\end{aligned}$$

where $\alpha_k(v)$, $\beta_k(v)$, and $\gamma_k(v)$ are polynomial functions of v. Referring to Peter's method [13], we define the polynomials as:

$$\begin{aligned}
&\alpha_k(v) = (1-v)\alpha_k(0) + v\alpha_k(1),\\
&\beta_k(v) = (1-v) + v,\\
&\gamma_k(v) = (1-v)^2\gamma_k(0) + v^2\gamma_k(1). \qquad (3.9)
\end{aligned}$$

By substituting Eqn. (3.9) into Eqn. (3.8), according to the degree elevation relation [3], the constraint condition of G^1-continuity is given anew by:

$$\begin{aligned}
&\alpha_k(0)\tilde{\mathbf{a}}_0^k + \tilde{\mathbf{b}}_0^k + \gamma_k(0)\tilde{\mathbf{c}}_0^k = 0,\\
&\alpha_k(0)\tilde{\mathbf{a}}_1^k + \tilde{\mathbf{b}}_1^k + \frac{1}{3}\left\{\alpha_k(1)\tilde{\mathbf{a}}_0^k + \tilde{\mathbf{b}}_0^k\right\} + \frac{2}{3}\gamma_k(0)\tilde{\mathbf{c}}_1^k = 0,\\
&\alpha_k(1)\tilde{\mathbf{a}}_1^k + \tilde{\mathbf{b}}_1^k + \alpha_k(0)\tilde{\mathbf{a}}_2^k + \tilde{\mathbf{b}}_2^k\\
&\quad + \frac{1}{3}\left\{\gamma_k(0)\tilde{\mathbf{c}}_2^k + \gamma_k(1)\tilde{\mathbf{c}}_0^k\right\} = 0,\\
&\alpha_k(1)\tilde{\mathbf{a}}_2^k + \tilde{\mathbf{b}}_2^k + \frac{1}{3}\left\{\alpha_k(0)\tilde{\mathbf{a}}_3^k + \tilde{\mathbf{b}}_3^k\right\} + \frac{2}{3}\gamma_k(1)\tilde{\mathbf{c}}_1^k = 0,\\
&\alpha_k(1)\tilde{\mathbf{a}}_3^k + \tilde{\mathbf{b}}_3^k + \gamma_k(1)\tilde{\mathbf{c}}_2^k = 0. \qquad (3.10)
\end{aligned}$$

From the first and the fifth equations in Eqn. (3.10) and the balance of coplanar three vectors, we have:

$$\begin{aligned}
&\alpha_k(0) = \frac{(\tilde{\mathbf{b}}_0^k \times \tilde{\mathbf{c}}_0^k)(\tilde{\mathbf{c}}_0^k \times \tilde{\mathbf{a}}_0^k)}{\left|\tilde{\mathbf{c}}_0^k \times \tilde{\mathbf{a}}_0^k\right|^2},\ \gamma_k(0) = \frac{(\tilde{\mathbf{a}}_0^k \times \tilde{\mathbf{b}}_0^k)(\tilde{\mathbf{c}}_0^k \times \tilde{\mathbf{a}}_0^k)}{\left|\tilde{\mathbf{c}}_0^k \times \tilde{\mathbf{a}}_0^k\right|^2},\\
&\alpha_k(1) = \frac{(\tilde{\mathbf{b}}_3^k \times \tilde{\mathbf{c}}_2^k)(\tilde{\mathbf{c}}_2^k \times \tilde{\mathbf{a}}_3^k)}{\left|\tilde{\mathbf{c}}_2^k \times \tilde{\mathbf{a}}_3^k\right|^2},\ \gamma_k(1) = \frac{(\tilde{\mathbf{a}}_3^k \times \tilde{\mathbf{b}}_3^k)(\tilde{\mathbf{c}}_2^k \times \tilde{\mathbf{a}}_3^k)}{\left|\tilde{\mathbf{c}}_2^k \times \tilde{\mathbf{a}}_3^k\right|^2}. \qquad (3.11)
\end{aligned}$$

To satisfy Eqn. (3.7) and Eqn. (3.10) simultaneously, we introduce the following two constraints:

$$\begin{aligned}
&\alpha_k(0) = \alpha_k(1) = \alpha\ (k = 1,2,\ldots,n),\\
&\gamma_k(1) = \gamma_{k+1}(0) = 0\ (k = 1,2,\ldots,n-1), \qquad (3.12)
\end{aligned}$$

where α is a constant scalar. From the first constraint of Eqn. (3.12), magnifications which are given to $\tilde{\mathbf{a}}_3^k$ to balance with $\tilde{\mathbf{b}}_3^k$ are constrained to α. Likewise, magnifications which are given to $\tilde{\mathbf{a}}_0^0$ to balance with $\tilde{\mathbf{b}}_0^0$ are also constrained to α. We determine α using partial derivative vectors of two offset surfaces at both ends of the common boundary. Let $\mathbf{a}_0$, $\mathbf{b}_0$, $\mathbf{c}_0$, $\mathbf{a}_1$, $\mathbf{b}_1$, and $\mathbf{c}_1$ be the partial derivative vectors that have same initial point and direction as $\mathbf{a}_0^1$, $\mathbf{b}_0^1$, $\mathbf{c}_0^1$, $\mathbf{a}_1^n$, $\mathbf{b}_1^n$, and $\mathbf{c}_1^n$, respectively. Since the offset surfaces are G^1-continuous, the following relations are obtained analogous to Eqn. (3.10).

$$\begin{aligned}
&\alpha_0\mathbf{a}_0 + \mathbf{b}_0 + \gamma_0\mathbf{c}_0 = 0,\\
&\alpha_1\mathbf{a}_1 + \mathbf{b}_1 + \gamma_1\mathbf{c}_1 = 0. \qquad (3.13)
\end{aligned}$$

If $\gamma_0 = \gamma_1 = 0$ and $\alpha_0 = \alpha_1 = -1$, two offset surfaces adjoin with C^1-continuity at both ends of the common boundary at least. Thus, we set α to

$$\alpha = \frac{1}{2}(\alpha_0 + \alpha_1) \qquad (3.14)$$

so that approximated surfaces adjoin with C^1-continuity in that case. From the second constraint of Eqn. (3.12), $\tilde{\mathbf{a}}_3^k$ and $\tilde{\mathbf{b}}_3^k (k = 1,2,\ldots,n-1)$ are restricted to same direction. We define the direction of $\tilde{\mathbf{a}}_3^k$ and $\tilde{\mathbf{b}}_3^k$ as an intermediate direction between $\mathbf{a}_3^k$ and $\mathbf{b}_3^k$ given by

$$\mathbf{V}_k = \frac{\mathbf{a}_3^k}{\left|\mathbf{a}_3^k\right|} + \frac{\mathbf{b}_3^k}{\left|\mathbf{b}_3^k\right|} \quad (k = 1,2,\ldots,n-1). \qquad (3.15)$$

3.3.2. *Adjusting control points according to constraint conditions*

We adjust control points of patches existing along the common boundary so that two adjacent patches on the common boundary are G^1-continuous and those

along the common boundary are C^1-continuous. Control points to be adjusted and constraint conditions to satisfy G^1- and C^1-continuity simultaneously are described in Section 3.3.1. First, we adjust control points on the common boundary (bold red dots in Fig. 6(a), i.e., $\mathbf{R}_1^k$, $\mathbf{R}_2^k$ $(k = 1, 2, \ldots, n)$ in Fig. 5). For $\tilde{\mathbf{R}}_1^1$ and $\tilde{\mathbf{R}}_2^1$, to retain directions of partial derivative vectors of the patches in the v direction at the end point of the common boundary, we introduce the constraint

$$\tilde{\mathbf{R}}_1^1 - \mathbf{R}_0^1 = \lambda_v(\mathbf{R}_1^1 - \mathbf{R}_0^1), \tag{3.16}$$

where λ_v is an unknown scalar. By substituting Eqn. (3.12) and $k = 1$ into Eqn. (3.10), the second equation in Eqn. (3.10) is expressed as follows according to the other four equations in Eqn. (3.10).

$$\tilde{\mathbf{c}}_0^1 + \tilde{\mathbf{c}}_2^1 - 2\tilde{\mathbf{c}}_1^1 = 0. \tag{3.17}$$

Since $\tilde{\mathbf{c}}_0^1 = \tilde{\mathbf{R}}_1^1 - \mathbf{R}_0^1$, $\tilde{\mathbf{c}}_1^1 = \tilde{\mathbf{R}}_2^1 - \tilde{\mathbf{R}}_1^1$, and $\tilde{\mathbf{c}}_2^1 = \mathbf{R}_3^1 - \tilde{\mathbf{R}}_2^1$, $\tilde{\mathbf{R}}_2^1$ is expressed with $\tilde{\mathbf{R}}_1^1$ from Eqn. (3.17).

$$\tilde{\mathbf{R}}_2^1 = \tilde{\mathbf{R}}_1^1 + \frac{1}{3}(\mathbf{R}_3^1 - \mathbf{R}_0^1). \tag{3.18}$$

From Eqns. (3.18) and (3.16), $\tilde{\mathbf{R}}_1^1$ and $\tilde{\mathbf{R}}_2^1$ are expressed by linear functions of λ_v. Therefore, we determine λ_v as follows using the least-squares method so that two control points move as little as possible (see APPENDIX for the derivation).

$$\lambda_v = \frac{1}{2} - \frac{(\mathbf{R}_1^1 - \mathbf{R}_0^1)(\mathbf{R}_3^1 + 2\mathbf{R}_0^1 - 3\mathbf{R}_2^1)}{6\left|\mathbf{R}_1^1 - \mathbf{R}_0^1\right|^2}. \tag{3.19}$$

$\tilde{\mathbf{R}}_1^1$ and $\tilde{\mathbf{R}}_2^1$ are given by substituting Eqn. (3.19) into Eqn. (3.16) and then substituting Eqn. (3.16) into Eqn. (3.18). In addition, $\tilde{\mathbf{R}}_1^2$ are given by substituting Eqn. (3.18) into Eqn. (3.7). $\tilde{\mathbf{R}}_1^n$, $\tilde{\mathbf{R}}_2^n$, and $\tilde{\mathbf{R}}_2^{n-1}$ are similarly calculated. For $\tilde{\mathbf{R}}_2^k$ and $\tilde{\mathbf{R}}_1^{k+1}$ $(k = 2, 3, \ldots, n-2)$, we calculate them using the method described in Section 3.2.

Next, we adjust control points existing beside the common boundary and belonging to the boundary curves of the patches in the u direction (bold red dots in Fig. 6(b), i.e., $\tilde{\mathbf{P}}_0^1$, $\tilde{\mathbf{Q}}_0^1$, $\tilde{\mathbf{P}}_3^k$, $\tilde{\mathbf{Q}}_3^k$ $(k = 1, 2, \ldots, n)$ in Fig. 5). For $\tilde{\mathbf{P}}_0^1$ and $\tilde{\mathbf{Q}}_0^1$, to retain the direction of the partial derivative of the patches in the u direction at the end of the common boundary, we introduce the following constraints:

$$\tilde{\mathbf{a}}_0^1 = \lambda_a \mathbf{a}_0^1, \tilde{\mathbf{b}}_0^1 = \lambda_b \mathbf{b}_0^1, \tag{3.20}$$

where λ_a and λ_b are unknown scalars. By substituting Eqns. (3.20) and (3.12) into Eqn. (3.11), λ_b is expressed as follows by a linear function of λ_a since $\tilde{\mathbf{c}}_0^1$ is known already.

$$\lambda_b = \frac{\alpha}{\hat{\alpha}}\lambda_a \text{ where } \hat{\alpha} = \frac{(\mathbf{b}_0^1 \times \tilde{\mathbf{c}}_0^1)(\tilde{\mathbf{c}}_0^1 \times \mathbf{a}_0^1)}{\left|\tilde{\mathbf{c}}_0^1 \times \mathbf{a}_0^1\right|^2}. \tag{3.21}$$

From Eqns. (3.20) and (3.21), $\tilde{\mathbf{P}}_0^1$ and $\tilde{\mathbf{Q}}_0^1$ are expressed by a linear functions of λ_a since $\tilde{\mathbf{a}}_0^1 = \mathbf{R}_0^1 - \tilde{\mathbf{P}}_0^1$ and $\tilde{\mathbf{b}}_0^1 = \tilde{\mathbf{Q}}_0^1 - \mathbf{R}_0^1$. Therefore, we determine λ_a as follows using the least-squares method so that two control points move as little as possible (see APPENDIX for the derivation).

$$\lambda_a = \frac{\hat{\alpha}^2\left|\mathbf{a}_0^1\right|^2 + \hat{\alpha}\alpha\left|\mathbf{b}_0^1\right|^2}{\hat{\alpha}^2\left|\mathbf{a}_0^1\right|^2 + \alpha^2\left|\mathbf{b}_0^1\right|^2}. \tag{3.22}$$

Substituting Eqns. (3.22) and (3.21) into Eqn. (3.20) yields $\tilde{\mathbf{P}}_0^1$ and $\tilde{\mathbf{Q}}_0^1$. $\tilde{\mathbf{P}}_3^n$ and $\tilde{\mathbf{Q}}_3^n$ are similarly calculated. For $\tilde{\mathbf{P}}_3^1$ and $\tilde{\mathbf{Q}}_3^1$, $\tilde{\mathbf{a}}_3^1$ and $\tilde{\mathbf{b}}_3^1$ are restricted to the direction defined by Eqn. (3.15). Then, $\tilde{\mathbf{a}}_3^1$ is given by

$$\tilde{\mathbf{a}}_3^1 = \lambda_u \mathbf{V}_1, \tag{3.23}$$

where λ_u is an unknown scalar. By substituting Eqn. (3.12) into Eqn. (3.10), $\tilde{\mathbf{b}}_3^1$ is expressed as follows

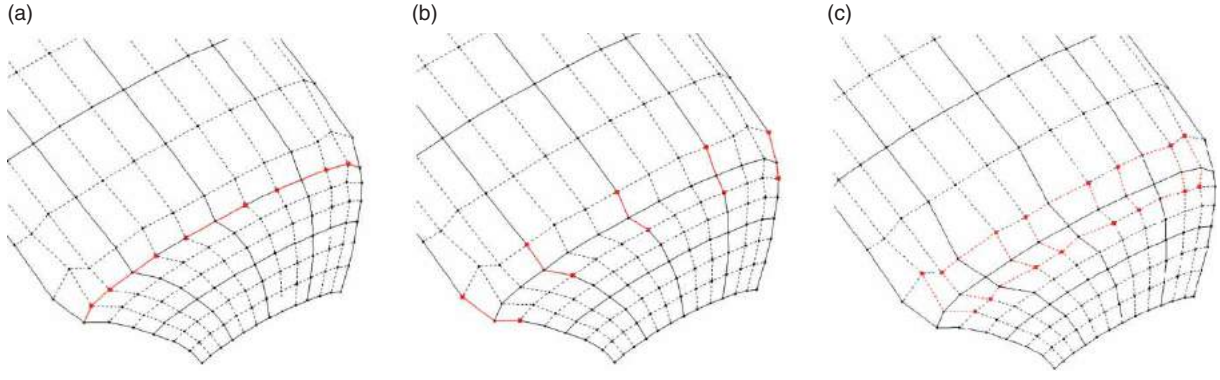

Fig. 6: (a) Control points on the common boundary, (b) Control points beside the common boundary, (c) Inner control points.

according to the fifth equation of Eqn. (3.10).

$$\tilde{\mathbf{b}}_3^1 = -\alpha\tilde{\mathbf{a}}_3^1. \tag{3.24}$$

From Eqns. (3.23) and (3.24), $\tilde{\mathbf{a}}_3^1$ and $\tilde{\mathbf{b}}_3^1$ are expressed by linear functions of λ_u. Therefore, we determine λ_u as follows using the least-squares method so that two control points move as little as possible (see APPENDIX for the derivation).

$$\lambda_u = \frac{\mathbf{V}_1\mathbf{a}_3^1 - \alpha\mathbf{V}_1\mathbf{b}_3^1}{(1+\alpha^2)\,|\mathbf{V}_1|^2}. \tag{3.25}$$

$\tilde{\mathbf{P}}_3^1$ and $\tilde{\mathbf{Q}}_3^1$ are given by Eqns. (3.25), (3.23) and (3.24) since $\tilde{\mathbf{a}}_3^1 = \mathbf{R}_3^1 - \tilde{\mathbf{P}}_3^1$ and $\tilde{\mathbf{b}}_3^1 = \tilde{\mathbf{Q}}_3^1 - \mathbf{R}_3^1$. $\tilde{\mathbf{P}}_3^k$ and $\tilde{\mathbf{Q}}_3^k (k = 2,\ldots,n-1)$ are similarly calculated.

Finally, we adjust the remaining inner control points (bold red dots in Fig. 6(c), i.e., $\tilde{\mathbf{P}}_1^k$, $\tilde{\mathbf{P}}_2^k$, $\tilde{\mathbf{Q}}_1^k$, $\tilde{\mathbf{Q}}_2^k$ $(k = 1,2,\ldots,n)$ in Fig. 5). For $\tilde{\mathbf{P}}_1^1$ and $\tilde{\mathbf{Q}}_1^1$, by substituting Eqn. (3.12) and $k = 1$ into Eqn. (3.10), the third equation in Eqn. (3.10) is expressed as follows according to the fourth and the fifth equations in Eqn. (3.10).

$$\alpha\tilde{\mathbf{a}}_1^1 + \tilde{\mathbf{b}}_1^1 + \frac{1}{3}\gamma_1(0)\tilde{\mathbf{c}}_2^1 = 0. \tag{3.26}$$

Since $\tilde{\mathbf{a}}_0^1$, $\tilde{\mathbf{b}}_0^1$, and $\tilde{\mathbf{c}}_0^1$ are already known, $\gamma_1(0)$ is given by Eqn. (3.11). Thus, $\tilde{\mathbf{Q}}_1^1$ is expressed by a linear function of $\tilde{\mathbf{P}}_1^1$ as follows from Eqn. (3.26) since $\tilde{\mathbf{a}}_1^1 = \tilde{\mathbf{R}}_1^1 - \tilde{\mathbf{P}}_1^1$, $\tilde{\mathbf{b}}_1^1 = \tilde{\mathbf{Q}}_1^1 - \tilde{\mathbf{R}}_1^1$, and $\tilde{\mathbf{c}}_2^1 = \mathbf{R}_3^1 - \tilde{\mathbf{R}}_2^1$.

$$\tilde{\mathbf{Q}}_1^1 = \tilde{\mathbf{R}}_1^1 - \alpha(\tilde{\mathbf{R}}_1^1 - \tilde{\mathbf{P}}_1^1) - \frac{1}{3}\gamma_1(0)(\mathbf{R}_3^1 - \tilde{\mathbf{R}}_2^1). \tag{3.27}$$

Therefore, we determine $\tilde{\mathbf{P}}_1^1$ as follows using the least-squares method so that two control points move as little as possible (see APPENDIX for the derivation).

$$\tilde{\mathbf{P}}_1^1 = \frac{\mathbf{P}_1^1 + \alpha\mathbf{Q}_1^1 + \alpha(\alpha-1)\tilde{\mathbf{R}}_1^1 + \alpha\gamma_1(0)(\mathbf{R}_3^1 - \tilde{\mathbf{R}}_2^1)/3}{1+\alpha^2}. \tag{3.28}$$

$\tilde{\mathbf{Q}}_1^1$ is given by substituting Eqn. (3.28) into Eqn. (3.27). $\tilde{\mathbf{P}}_2^n$ and $\tilde{\mathbf{Q}}_2^n$ are similarly calculated. For $\tilde{\mathbf{P}}_2^1$, $\tilde{\mathbf{Q}}_2^1$, $\tilde{\mathbf{P}}_1^2$, and $\tilde{\mathbf{Q}}_1^2$ (which are four inner control points adjacent to the point at which corners of four patches converge), by substituting Eqn. (3.12) into Eqn. (3.10), the following simultaneous equations are given from Eqns. (3.10) and (3.7) since $\tilde{\mathbf{R}}_1^2$, $\tilde{\mathbf{R}}_2^1$, $\tilde{\mathbf{P}}_3^1$, and $\tilde{\mathbf{Q}}_3^1$ are known.

$$\begin{bmatrix} \alpha & -1 & 0 & 0 \\ 1 & 0 & \nu_1 & 0 \\ 0 & 0 & \alpha & -1 \\ 0 & 1 & 0 & \nu_1 \end{bmatrix} \begin{bmatrix} \tilde{\mathbf{P}}_1^2 \\ \tilde{\mathbf{Q}}_1^2 \\ \tilde{\mathbf{P}}_2^1 \\ \tilde{\mathbf{Q}}_2^1 \end{bmatrix} = \begin{bmatrix} (\alpha-1)\tilde{\mathbf{R}}_1^2 \\ (\nu_1+1)\tilde{\mathbf{P}}_3^1 \\ (\alpha-1)\tilde{\mathbf{R}}_2^1 \\ (\nu_1+1)\tilde{\mathbf{Q}}_3^1 \end{bmatrix}. \tag{3.29}$$

However, the solution of Eqn. (3.29) is indefinite because of rank deficiency. On the other hand, $\tilde{\mathbf{Q}}_2^1$, $\tilde{\mathbf{P}}_1^2$, and $\tilde{\mathbf{Q}}_1^2$ are expressed by linear functions of $\tilde{\mathbf{P}}_2^1$ from Eqn. (3.29). Therefore, we determine $\tilde{\mathbf{P}}_2^1$ as follows using the least-squares method so that four control points move as little as possible (see APPENDIX for the derivation).

$$\tilde{\mathbf{P}}_2^1 = \frac{\begin{array}{c}\mathbf{P}_2^1 + \alpha\mathbf{Q}_2^1 - \nu_1\tilde{\mathbf{P}}_1^2 - \alpha\nu_1\tilde{\mathbf{Q}}_1^2 + \alpha(\alpha-1)(\tilde{\mathbf{R}}_2^1 - \nu_1\tilde{\mathbf{R}}_1^2) \\ +\nu_1(\nu_1+1)(1+\alpha^2)\tilde{\mathbf{P}}_3^1\end{array}}{1+\alpha^2+\nu_1^2+\alpha^2\nu_1^2}. \tag{3.30}$$

$\tilde{\mathbf{Q}}_2^1, \tilde{\mathbf{P}}_1^2$, and $\tilde{\mathbf{Q}}_1^2$ are calculated by substituting Eqn. (3.30) into Eqn. (3.29). Remaining each of the four inner control points adjacent to the point at which corners of four patches converge are similarly calculated.

As the result, two patches adjacent on the common boundary are G^1-continuous and those along the common boundary are C^1-continuous. Then, using the method described in Section 3.2, we measure errors of boundary curves of these patches and interior of these patches, and subdivide parameter domains of the offset surfaces if the patches that do not satisfy the tolerance are detected. After that, using the method described in Section 3.2 and 3.3.2, we reconstruct patches repeatedly until all patches satisfy the tolerance.

4. EXAMPLES

Fig. 7 is an example of applying the technique described in this paper. Fig. 7(a) shows a three-dimensional model in the shape of bottles. Fig. 7(b) shows two G^1-continuous bicubic Bezier surfaces of the model. The distance between end points of the common boundary is 80.0. We applied our technique to the surfaces. Fig. 7(c) shows the result. Fig. 7(d) is other view of Fig. 7(c). The offset distance is 5.0, the tolerances for boundary curves of patches and interior of patches are 0.1, and the angle tolerance is 1.0 degree. Fig. 7(e) shows the sample points used to generate the approximated offset surfaces rendered in Fig. 7(c),(d). The blue dots are the sample points used to calculate the inner control points of patches in the

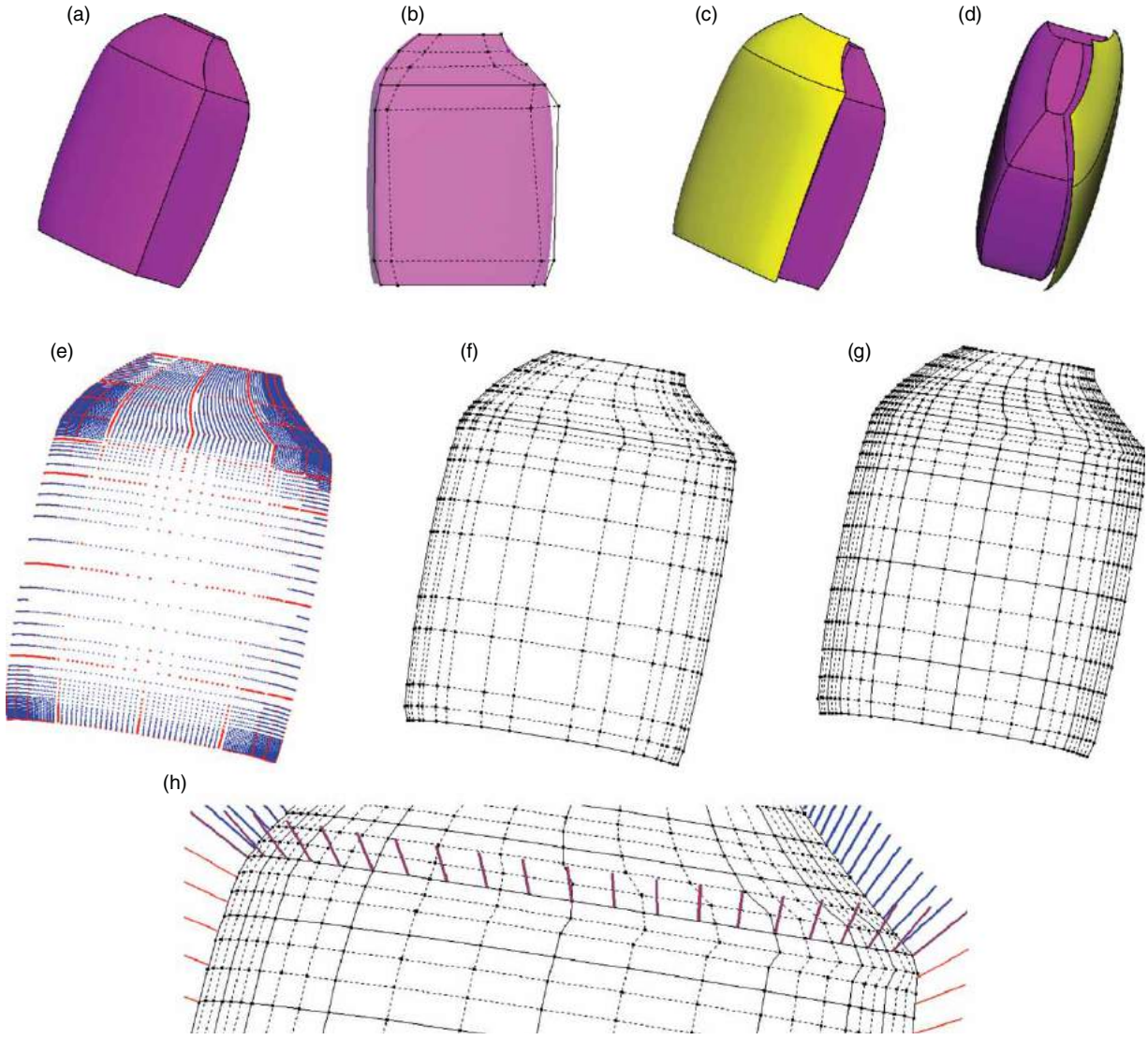

Fig. 7: (a) A bottle shape, (b) Two G^1-continuous surfaces, (c) The result, (d) Another view of (c), (e) Sample points, (f) Control points for (c), (g) Bicubic Bezier patches for (f), (h) Enlarged view of (g) with normal vectors.

approximated surface. The red dots are the sample points used to calculate control points on boundary curves of the patches. Fig. 7(f) shows the control points of the approximated offset surfaces rendered in Fig. 7(c), (d). Fig. 7(g) shows the bicubic Bezier patches which are combined to two bicubic B-spline surfaces depicted in Fig. 7(f). As understood from comparison between Fig. 7(f) and Fig. 7(g), each bicubic B-spline surface in Fig. 7(g) has no control points on boundary curves of the patches because those are C^1-continuous. Fig. 7(h) is the enlarged view of the bicubic Bezier patches of Fig. 7(g) along the common boundary, and shows normal vectors of the approximated offset surfaces along the boundary curves. As shown in Fig. 7(h), no gaps and creases appear between two surfaces because the patches adjoin to be one-on-one along the common boundary and those are G^1-continuous.

Fig. 8 is another example. Fig. 8(a) shows a three-dimensional model in the shape of levers. Fig. 8(b) shows two G^1-continuous bicubic Bezier surfaces of the model. The distance between end points of the common boundary is about 63.3. Fig. 8(c) is another view of Fig. 8(b). We applied our technique to the surfaces. Fig. 8(d) shows the result. The offset distance is 5.0, the tolerances for boundary curves of patches and interior of patches are 0.1, and the angle tolerance is 1.0 degree. Fig. 8(e) shows the sample points used to generate the approximated offset surfaces rendered in Fig. 8(d). The meanings of color of the sample points are same as the previous example. Fig. 8(f) shows the control points of the approximated offset surfaces rendered in Fig. 8(c), (d). Fig. 7(g) shows the bicubic Bezier patches which are combined to two bicubic B-spline surfaces depicted in Fig. 8(f). As understood from comparison between Fig. 8(f) and

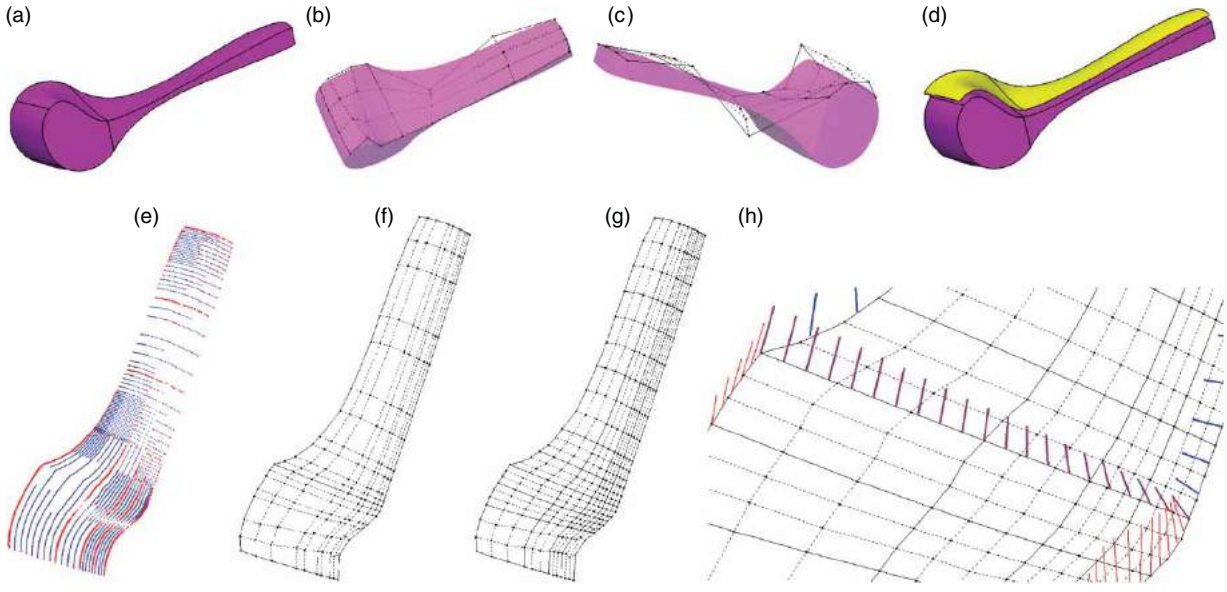

Fig. 8: (a) A lever shape, (b) Two G^1-continuous surfaces, (c) Another view of (b), (d) The result, (e) Sample points, (f) Control points for (d), (g) Bicubic Bezier patches for (f), (h) Enlarged view of (g) with normal vectors.

Fig. 8(g), each bicubic B-spline surface in Fig. 8(g) has no control points on boundary curves of the patches because those are C^1-continuous. Fig. 8(h) is the enlarged view of the bicubic Bezier patches of Fig. 8(g) along the common boundary, and shows normal vectors of the approximated offset surfaces along the boundary curves. As shown in Fig. 8(h), no gaps and creases appear between two surfaces because the patches adjoin to be one-on-one along the common boundary and those are G^1-continuous.

On a PC with Intel(R) Core(TM)2 Duo 2.2 GHz CPU and 2 GB RAM, the processing time is about 4.0 seconds in the case of Fig. 7 and is about 1.8 seconds in the case of Fig. 8. Our technique could run at a practical speed although it may be somewhat bovine because of a lot of sample points marked in Fig. 7(e) and Fig. 8(e).

5. CONCLUSION

This paper proposed a technique for approximating two G^1-continuous offset surfaces. The technique generates two G^1-continuous approximated surfaces represented by C^1-continuous bicubic B-spline surfaces. The approximated surfaces are higher quality than generated using existing methods, because our technique avoids gaps or creases between the surfaces with the following two ideas: (1) subdivide parameter domains of offset surfaces so that the patches along the common boundary adjoin each other to be one-on-one on the common boundary, and ensure the shapes of two boundary curves on the common boundary between two patches adjoining each other are same, and (2) use the original constraint conditions to control points of the patches along the common boundary to satisfy G^1- and C^1-continuity simultaneously. Furthermore, because our approximated surfaces are C^1-continuous, those are tractable in numerical calculation of first order differential equations, such as trace calculations for blending surfaces or tracing intersection between surfaces.

REFERENCES

[1] Bastl, B.; Juttler, B.; Kosinka, J.; Lavicka, M.: Computing exact rational offsets of quadratic triangular Bezier surface patches, Computer-Aided Design, 40(2), 2008, 197-209, DOI:10.1016/j.cad.2007.10.008.

[2] Beeker, E.: Smoothing of shapes designed with free-form surfaces, Computer-Aided Design, 18(4), 1986, 224-232, DOI:10.1016/0010-4485(86)90134-X.

[3] Du, W.-H.; Schmitt, F.-J.-M.: On the G^1 continuity of piecewise Bezier surfaces: a review with new results, Computer-Aided Design, 22(9), 1990, 556-573, DOI:10.1016/0010-4485(90)90041-A.

[4] Farouki, R.-T.: The approximation of non-degenerate offset surfaces, Computer-Aided Geometric Design, 3(1), 1986, 15-43, DOI:10.1016/0167-8396(86)90022-1.

[5] Farouki, R.-T.; Sverrisson, R.: Approximation of rolling-ball blends for free-form parametric surfaces, Computer-Aided Design, 28(11), 1996, 871-878, DOI:10.1016/0010-4485(96)00008-5.

[6] Hermann, T.: On the smoothness of offset surfaces, Computer-Aided Geometric Design, 15(5), 1998, 529-533, DOI:10.1016/S0167-8396(98)00002-8.

[7] Hoschek, J.; Schneider, F.; Wassum, P.: Optimal approximate conversion of spline surfaces, Computer-Aided Geometric Design, 6(4), 1989, 293-306, DOI:10.1016/0167-8396(89)90030-7.

[8] ISO 1660:1987 Technical drawings – Dimensioning and tolerancing of profiles, International Organization for Standardization, 1987.

[9] ISO 10303-59:2008 Industrial automation systems and integration – Product data representation and exchange – Part 59: Integrated generic resource – Quality of product shape data, International Organization for Standardization, 2008.

[10] Kikuchi, Y.; Hiraoka, H.; Otaka, A.; Tanaka, F.; Kobayashi, K.; Soma, A.: PDQ (Product Data Quality): Representation of Data Quality for Product Data and Specifically for Shape Data, Transactions of the ASME, 10(2), 2010, 021003(8 pages), DOI:10.1115/1.3402615.

[11] Maekawa, T.: An overview of offset curves and surfaces, Computer-Aided Design, 31(3), 1999, 165-173, DOI:10.1016/S0010-4485(99)00013-5.

[12] Patrikalakis, N.M.: Surface-to-surface intersections, Computer Graphics and Applications, IEEE, 13(1), 1993, 89-95, DOI:10.1109/38.180122.

[13] Peters, J.: Patching Catmull-Clark meshes, ACM Computer Graphics SIGGRAPH, 2000, 255-258, DOI:10.1145/344779.344908.

[14] Piegl, L.; Tiller, W.: Computing offsets of NURBS curves and surfaces, Computer-Aided Design, 31(2), 1999, 147-156. DOI:10.1016/S0010-4485(98)00066-9.

[15] Piegl, L.; Tiller, W.: The NURBS Book, Springer, New York, 1997, DOI:10.1007/978-3-642-59223-2.

APPENDIX

Let $\mathbf{P}_i (i = 1, 2, \ldots, n)$ be control points to be adjusted and constrained by each other. Let $\tilde{\mathbf{P}}_i$ be the control points after adjustment, the condition to minimize the sum of distance to be moved δ is given by

$$\delta = \sum_{i=1}^{n} \left| \tilde{\mathbf{P}}_i - \mathbf{P}_i \right|^2 \rightarrow \min. \tag{A.1}$$

If $\tilde{\mathbf{P}}_2$, $\tilde{\mathbf{P}}_3$, …, and $\tilde{\mathbf{P}}_n$ are linear functions of $\tilde{\mathbf{P}}_1$, δ is a quadratic function of $\tilde{\mathbf{P}}_1$. Therefore, $\tilde{\mathbf{P}}_1$ satisfying Eqn. (A.1) is obtained by solving

$$\frac{d\delta}{d\tilde{\mathbf{P}}_1} = 0. \tag{A.2}$$

If $\tilde{\mathbf{P}}_1$, $\tilde{\mathbf{P}}_2$, …, and $\tilde{\mathbf{P}}_n$ are linear functions of an unknown scalar λ, δ is a quadratic function of λ. Therefore, λ satisfying Eqn. (A.1) is obtained by solving

$$\frac{d\delta}{d\lambda} = 0. \tag{A.3}$$